Copyright © 2014 Tech Science Press CMES, vol.101, no.6, pp.387-419, 2014

A Hybrid Variational Formulation for Strain Gradient Elasticity Part I: Finite Element Implementation

N. A. Dumont[1] **and D. Huamán**[1]

Abstract: The present paper starts with Mindlin's theory of the strain gradient elasticity, based on three additional constants for homogeneous materials (besides the Lamé's constants), to arrive at a proposition made by Aifantis with just one additional parameter. Aifantis' *characteristic material length* g^2, as it multiplies the Laplacian of the Cauchy stresses, may be seen as a penalty parameter to enforce interelement displacement gradient compatibility also in the case of a material in which the microstructure peculiarities are in principle not too relevant, but where high stress gradients occur. It is shown that the hybrid finite element formulation – as proposed by Pian and generalized by Dumont for finite and boundary elements – provides a natural conceptual framework to properly deal with the interelement compatibility of the normal displacement gradients, in which "corner nodes" are not an issue. Nonsingular fundamental solutions – domain interpolation functions – are presented for two-dimensional (2D) and three-dimensional (3D) problems, with the generation of families of finite elements that may be implemented in a straightforward way. Since the experimental data available in the technical literature are still scarce and the numerical results are in part questionable, consistency is assessed by means of patch tests and by investigating the spectral properties of the matrices derived for some 2D plane strain elements. The present developments, although of academical relevance, involve too many degrees of freedom to be considered for practical applications and are actually intended as a step toward a boundary-only implementation in terms of singular fundamental solutions.

Keywords: Gradient elasticity, variational methods, Hellinger-Reissner potential, hybrid finite element.

1 Introduction

The mathematical modeling of microdevices, in which structure and microstructure have approximately the same scale of magnitude, as well as of macrostructures of

[1] PUC-Rio – Pontifical Catholic University of Rio de Janeiro, Brazil.

markedly granular or crystal nature (microcomposites), demands a nonlocal approach for strains and stresses.

In no detriment to developments due to other researchers [Cosserat and Cosserat (1909); Toupin (1962); Ericksen and Trusdel (1958)], Mindlin's works in the 1960s [Mindlin (1964); Mindlin and Eshel (1968)] may be accounted the basis of the strain gradient theory. It has recently become the subject of a large number of analytical and experimental investigations motivated by the development of new structural materials together with the increasing use of micromechanical devices in the industry. Starting in the 1990s, Aifantis (2009, 2011) and coworkers managed to develop a simplified strain gradient theory based on only one additional elasticity constant, which opened up a series of interesting practical applications [Peerlings and Fleck (2004); Maranganti and Sharma (2007); Nikolov, Han, and Raabe (2007)]. On the other hand, developments that take into account nonlocal residuals by means of an integral operator were proposed in the 1970s [Eringen (1972)] and have been ever since the subject of investigation [Sciarra (2009)].

The stress gradient around crack and notch tips has also been recently studied in the closely related framework of dipolar gradient elasticity [see Grentzelou and Georgiadis (2008); Gourgiotis and Georgiadis (2009); Gourgiotis, Sifnaiou, and Georgiadis (2010) and references in there]. On the other hand, the general nonlocal effects in an elastic medium can be efficiently investigated by means of meshless methods, such as proposed by Sellountos, Tsinopoulos, and Polyzos (2012) in terms of a local boundary integral equation method. In this regard, the paper by Tang, Shen, and Atluri (2003) is remarkable, as the proposed developments seem to be simple to implement and allow for generalized non-classical stress-strain relations (several material constants, besides the Lamé's ones, as in Mindlin's seminal papers in the 1960s), by making use of only displacement quantities, with by far less degrees of freedom than in a finite element implementation (as in the present paper). However, the determination of the additional material properties for a practical application is still an unsurmountable experimental issue [Maranganti and Sharma (2007)], not to mention the task (from the mechanical, not the numerical, point of view) of considering appropriate non-classical boundary conditions.

Some recent works done by Beskos and collaborators have largely extended the field of applications of Aifantis' propositions [Tsepoura, Papargyri, Polyzos, and Beskos (2002); Polyzos, Tsepoura, Tsinopoulos, and Beskos (2003); Papargyri-Beskou, Polyzos, and Beskos (2009); Papargyri-Beskou and Beskos (2009); Tsinopoulos, Polyzos, and Beskos (2012)]. Ever since Toupin and Mindlin's time, investigations have been under development to establish the variational basis of the theory and to formulate equilibrium and kinematic boundary conditions consistently [Amanatidou and Aravas (2002); Giannakopoulos, Amanatidou, and Aravas

(2006)]. The non-singular formulation for 2D and 3D elasticity problems [Amanatidou and Aravas (2002), Zervos, Papanicolopulos, and Vardoulakis (2009)] has also been developed, which enables the construction of hybrid finite and boundary element families of general shape and number of degrees of freedom, as already done in the classical elasticity [Dumont (2003); Dumont and Prazeres (2005); Dumont (2005, 2007)]. All these formulations are the subject of the present investigations, including conceptual studies of the simplest conceivable rod, beam and 2D finite elements implementations, as a sequel of the works done by Dumont and Huamán (2009, 2010b). Although all developments can be readily extended to the frequency-domain analysis of time-dependent problems, the present outline is restricted to the static analysis, which actually involves the most relevant concepts.

This first paper reviews some basic aspects of the strain gradient theory of elasticity, as proposed by Aifantis and endorsed by the immense community of Greek researchers (as briefly reviewed above and which seem to be dominating this research field), and develops a formulation in the framework of the Hellinger-Reissner potential, which is the basis for a two-field numerical approach, with assumed stresses in the domain that satisfy a priori all static conditions, and a displacement field on the boundary, by means of which all boundary conditions must be fulfilled. In this paper, the domain stress field is approximated by non-singular functions, thus leading to a hybrid finite element method, similarly to what has been proposed by Pian several decades ago, although in a complete general framework.

Since nodal displacement gradients and double forces must be represented in the implemented finite elements, this formulation ends up with a large number of degrees of freedom, which is at least not very elegant. However, such a formulation has some academic value, since it allows drawing a series of conceptual conclusions in the spectral analyses and in the convergence tests performed. A theoretical counterpart of this paper – Part II – is being finished for publication, in which the stress field is approximated by singular fundamental solutions [Polyzos, Tsepoura, Tsinopoulos, and Beskos (2003)], thus leading to a boundary element implementation, which demands by far less degrees of freedom than in the finite element case. This boundary element formulation involves sophisticated numerical integration tools and requires some conceptual interpretations of the involved nodal parameters as well as of the ensuing numerical singularities to deserve being handled separately.

Sections 2 – 4 are in principle applicable to either a finite or a boundary element implementation. Some relevant remarks are accrued in the accompanying paper. Section 2 briefly lays out the proposed gradient theory of elasticity and prepares the ground for the subsequent developments. Section 3.1 details the requirements for a domain stress field and Section 3.2 describes the assumed displacements on

the boundary. The Hellinger-Reissner potential is applied in Section 4 as split into two virtual work statements in order to best clarify the proposed developments – the minutious sequence of equations seems necessary for the understanding not only of the present paper but also of any subsequent paper on this subject area. These developments are illustrated in Section 5 for the simplest cases of truss and beam elements (although a conceptual restriction applies to the latter kind of formulation), when already some theoretical conclusions are drawn. Finally, the application to 2D and 3D finite elements is discussed in Section 6, with some 2D numerical applications presented in Section 7.

2 Problem Formulation

Throughout this paper, repeated indices stand for summation and $(\,)_{,i}$ denotes a derivative with respect to the *i-th* coordinate direction. Following equations are given by Aifantis as a development of Mindlin's work:

$$\overline{\epsilon}_{ij} = \epsilon_{ij} + c_\epsilon \nabla^2 \epsilon_{ij}; \quad \overline{\sigma}_{ij} = \sigma_{ij} + c_\sigma \nabla^2 \sigma_{ij}; \quad \overline{\sigma}_{ij} = \lambda \overline{\epsilon}_{kk} \delta_{ij} + 2\mu \overline{\epsilon}_{ij} \tag{1}$$

where, quoting Aifantis (2009), "$(\sigma_{ij}, \epsilon_{ij})$ denote the stress and strain tensors for elastic deformation. The quantities (λ, μ) are the usual Lamé constants. The gradient coefficients c's are new phenomenological coefficients. ... (In fact, the simplest form of gradient elasticity theory corresponds to the case $c_\sigma = 0$)."

Independently from Mindlin's works, a *nonlocal elasticity* theory [Eringen (1972)] has also been developed, in which the stress field (in equilibrium with applied forces in the domain Ω) is expressed in terms of a nonlocal attenuation function $\alpha(|\mathbf{x} - \mathbf{x}'|, \tau)$, which incorporates into the constitutive equations the nonlocal effects at the reference point $\mathbf{x}$ produced by local strain at the source $\mathbf{x}'$, as

$$\sigma_{ij}(\mathbf{x}) = \int_\Omega \alpha(|\mathbf{x} - \mathbf{x}'|, \tau) C_{ijkl} \epsilon_{kl}(\mathbf{x}') \mathrm{d}\Omega \tag{2}$$

where C_{ijkl} is the elastic module tensor of the classical isotropic elasticity, $|\mathbf{x} - \mathbf{x}'|$ is the Euclidean distance, and τ is a material property that depends on external and internal characteristic lengths (Eringen's notation). According to Challamel and Wang (2008), Eq. (1) represents "*gradient elastic models* (the stress is defined explicitly from the local strain and its derivatives", whereas Eq. (2) represents "integral elastic models (the stress is obtained implicitly from an integral operator of the local strain)". Moreover, "(g)radient models can be considered as a 'weakly' nonlocal model, whereas (the) integral elastic model can be classified as (a) 'strongly' nonlocal model".

In either gradient or nonlocal formulation, the crucial issue is the determination of the material characteristic length(s). When consistently applied, both formulations

should lead to similar results. In fact, there may be no strict differentiation between the formulations when it comes to a computational implementation [Reddy (2007)]. It is worth pointing out two basic requirements that a gradient or nonlocal formulation should fulfill for consistency:

1. As proposed by Mindlin in the energy statements for a general 3D problem, the variation of the normal component $n_j u_{i,j}$ of the displacement gradient is independent of the variation of u_i on the boundary, with double tractions T_{ij} performing virtual work along Γ on the normal gradient variation

$$n_j n_l \delta u_{i,l} \equiv \delta u_{i,j} - (\delta_{jl} - n_j n_l)\delta u_{i,l} \tag{3}$$

   In this equation, n_i are the Cartesian projections of the outward unit normal to Γ and δ_{jl} is the Kronecker delta. A mechanical interpretation of the non-symmetric tensor T_{ij}, including its correlation with the Cosserat couple-stress vector, is given by Mindlin (1964).

2. A constant strain state must yield the same results of the classical elasticity [Sciarra (2009)]. This requirement has not been observed by some researchers, with inconsistent results.

Moreover, consistency of the formulation for applied rigid body displacements as well as for simple displacement fields (patch tests) should be checked, as done in the present paper. The implementation of the formulation in terms of finite elements is also not straightforward, as unique relations between local and global non-classical quantities must be ensured. These issues are dealt with later on in the paper.

3 Basic assumptions for a two-field variational implementation

3.1 Stress assumption in the domain

The stresses are approximated in the domain Ω of a generic 3D elastic body by the Cauchy stress τ^s_{ij} and the double stress μ^s_{kij}, with the superscript $()^s$ standing for *stress assumption*. For the sake of checking equilibrium, τ^s_{ij} and μ^s_{kij} are split into two parts, $\tau^s_{ij} = \tau^*_{ij} + \tau^p_{ij}$ and $\mu^s_{kij} = \mu^*_{kij} + \mu^p_{kij}$, where the superscript $()^*$ denotes the homogeneous solution of the differential equilibrium equation and the superscript $()^p$ stands for some arbitrary, particular solution for the applied body force f_i defined per unit volume in Ω. No "body double force" is prescribed [see Amanatidou and Aravas (2002)]. All quantities are supposed to vary in Ω as functions of the coordinates x, y, z. Except for analyticity, no concern is made at present about equilibrium on parts of the boundary Γ where forces are prescribed. According to the

technical literature on the gradient elasticity, one defines the tensor of total stresses

$$\sigma^s_{ij} = \tau^s_{ij} - \mu^s_{kij,k} \tag{4}$$

where τ^s_{ij} is the Cauchy stress tensor and $\mu^s_{kij,k}$ is the *double* stress tensor. This definition will be arrived at naturally in the frame of the virtual work statement below, as well as the equilibrium statement:

$$\sigma^s_{ji,j} + f_i = 0 \quad \text{in } \Omega \tag{5}$$

σ^s_{ij}, τ^s_{ij} and μ^s_{kij} are symmetric with respect to the directions i and j. According to Aifantis' proposition, the double stress tensor is related to the Cauchy stress tensor by means of the *material characteristic length* g^2:

$$\mu^s_{kij} = g^2 \tau^s_{ij,k} \quad \Rightarrow \quad \sigma^s_{ij} = \tau^s_{ij} - g^2 \tau^s_{ij,kk} \tag{6}$$

This stress field description for the gradient elasticity corresponds to a "Type II" description of three equivalent forms of the strain energy density [Mindlin and Eshel (1968); Amanatidou and Aravas (2002)]. The present notation is a simplified version of the notation proposed by Mindlin and Eshel, with the equivalences $\tau^s_{ij} \equiv \overline{\sigma}^s_{ij}$ and $\mu^s_{kij} \equiv \hat{\mu}_{kij}$. The strain field corresponding to τ^s_{ji} is $\epsilon^s_{ij} = \frac{1}{2}(u^s_{i,j} + u^s_{j,i}) \equiv \epsilon_{ij}$, and the strain gradient corresponding to μ^s_{kji} is $\frac{1}{2}(u^s_{i,jk} + u^s_{j,ik}) = \hat{\kappa}_{kij}$.

3.1.1 Stress fundamental solution

The stresses τ^s_{ij} are approximated in Ω, in the frame of the present variational formulation, by the sum of a sufficiently large number of "fundamental solutions" τ^*_{ijm} plus a particular solution:

$$\tau^s_{ij} = \tau^*_{ijm} p^*_m + \tau^p_{ij} \tag{7}$$

such that the equilibrium Eq. (5) is satisfied a priori for all p^*_m. Consequently, the double stresses μ^s_{kij} as well as the total stresses σ^s_{ij} become

$$\mu^s_{kij} = \mu^*_{kijm} p^*_m + \mu^p_{kij} \tag{8}$$

$$\sigma^s_{ij} = \sigma^*_{ijm} p^*_m + \sigma^p_{ij} \tag{9}$$

The parameters p^*_m are context-dependent in a general formulation, as developed by the authors in the frame of a finite element implementation [Dumont and Huamán (2009, 2010a,b)]. When using singular fundamental solutions, as presented in the companion paper, the set of n^* parameters p^*_m correspond to point forces applied along the boundary of the elastic body. For a finite element implementation, they are just some parameters multiplying polynomial or Bessel terms, as shown in Section 6.

3.1.2 Displacement fundamental solution

Displacement solutions u_i^s are obtained from τ_{ij}^s, μ_{kij}^s in terms of the fundamental solutions of Eq. (7) and of the particular solution τ_{ij}^p, μ_{kij}^p,

$$u_i^s = u_{im}^* p_m^* + u_i^p + u_i^r \quad \text{in } \Omega \tag{10}$$

which formally include a set u_i^r of rigid-body displacements. This explicit expression of the rigid body displacements may be omitted in the above equation with no conceptual harm, as they are implicitly included as an arbitrary amount of the particular solution u_i^p.

According to Eq. (10), a portion of the elastic body whose outward unit normal is n_j has as displacement gradient ($u_{i,j}^r \neq 0$ in the case of rigid-body rotation):

$$q_i^s = n_j \left(u_{im}^* p_m^* + u_i^p + u_i^r \right)_{,j} \quad \text{in } \Omega \tag{11}$$

3.2 Displacement assumption on the boundary

The displacements are approximated on Γ by an independent field u_i^d, where the superscript $()^d$ stands for *displacement assumption*. u_i^d satisfies the required boundary continuity conditions, that is, $u_i^d = \overline{u}_i$ on part Γ_u of the boundary with prescribed displacement $\overline{u}_i$. This is the only requirement on u_i^d that is made in the present frame of the Hellinger-Reissner potential. Except for analyticity, no assumption is explicitly made for the displacement u_i^d in Ω whether or not concerning gradient elasticity. According to the requirement number (1) in Section 2, a normal gradient field q_i^d must be postulated on Γ independently from $u_{i,j}^d n_j$ (which is actually not defined) and such that $q_i^d = \overline{q}_i$ on part Γ_q of the boundary with prescribed normal gradients $\overline{q}_i$ and also provided that interelement compatibility is satisfied. Then, for the geometry of Γ described in terms of the parametric variables (ξ, η),

$$\left.\begin{aligned} u_i^d &\equiv u_i^d(\xi,\eta) = u_{in}(\xi,\eta) d_n \equiv u_{in} d_n \\ q_i^d &\equiv q_i^d(\xi,\eta) = q_{i\ell}(\xi,\eta) q_\ell \equiv q_{i\ell} q_q \end{aligned}\right\} \quad \text{on } \Gamma \tag{12}$$

where u_{in} and $q_{i\ell}$ are interpolation functions of a total of n^d parameters d_n and q_q (not to be confounded with q_i). These nodal displacements and normal displacement gradients are – together with p_m^* of Eq. (7) – the primary unknowns of the variational problem. The set of functions u_{in} is used to interpolate both displacements (through the components u_x^d, u_y^d and u_z^d) and geometry data (through the coordinates x, y and z) along each subregion of Γ (a "boundary element", or, more adequately, a *boundary segment*) in the present variational context – consistently with the isoparametric description of the body's geometry. The interpolation functions

$q_{i\ell}$, used to interpolate normal displacement gradients (through the components q_x^d, q_y^d and q_z^d), may be different from u_{in}. In the case of non-smooth surfaces, the nodal parameters q_ℓ must be independently prescribed for each normal direction of the surfaces adjacent to a node.

4 The Hellinger-Reissner potential applied to gradient elasticity

In the next Sections, the Hellinger-Reissner potential [Dumont (1989)] is split into two virtual work principles in order to clarify the conceptual aspects affected by the gradient elasticity. This Section basically repeats the initial outline by Dumont and Huamán (2010a,b), although some relevant remarks are added. The two-field assumptions of Sections 3.1 and 3.2 are the starting point to develop all matrix equations in terms of n^* and n^d stress and displacement parameters.

4.1 Displacement virtual work for equilibrium checking

The following statement is found in similar form in several developments on gradient elasticity as $\delta W^{\text{int}} = \delta W^{\text{ext}}$. Mindlin and Eshel (1968) as well as Amanatidou and Aravas (2002), for instance, imply with this expression the equivalence of the variation of internal and external works, in terms of virtual displacements that should be referred to herein as δu_i^s. However, in the present context, $\delta u_i^s \neq \delta u_i^d$ on Γ, besides the fact that u_i^d is not defined in Ω (except for the trivial cases of truss and beam elements [Dumont and Huamán (2009)]).

Equilibrium of the stress field is weakly enforced by means of the displacement virtual work statement

$$\int_\Omega \left(\tau_{ji}^s \delta u_{i,j}^d + \mu_{kji}^s \delta u_{i,jk}^d\right) \mathrm{d}\Omega = \int_\Omega f_i \delta u_i^d \mathrm{d}\Omega + \int_\Gamma P_i \delta u_i^d \mathrm{d}\Gamma + \int_\Gamma Q_{is} \delta u_{i,s}^d \mathrm{d}\Gamma + \int_\Gamma R_i \delta q_i^d \mathrm{d}\Gamma \tag{13}$$

In the terms on the right-hand side of the above equation, f_i and P_i are *classical* body forces and boundary tractions, respectively, which perform virtual work on displacements, as indicated, whereas R_i and Q_{is} are *normal* and *tangential* double tractions. In the latter expression as well as in the tangential displacement gradient $\delta u_{i,s}^d$, the subscript s refers to the natural coordinates that describe the boundary surface: ξ for a 2D problem or (ξ, η) for a 3D problem. The *normal double* traction forces

$$R_i = T_{ji} n_j = \mu_{kji}^s n_k n_j \tag{14}$$

perform virtual work on normal displacement gradients $\delta q_i \equiv n_l \delta u_{i,l}$. The relation of the *tangential* double tractions Q_{is} with the internal stress field is elucidated at

the end of this Section. The application of R_i and Q_{is} as Neumann boundary conditions is not a simple matter. These static quantities are investigated later on by means of some numerical examples.[1] The boundary integrals are expressed as if plain Neumann conditions are applied. However, Eq. (13) is consistent and general, as $\delta u_i^d = 0$ and $\delta q_i^d = 0$ wherever such displacement quantities are prescribed in a numerical problem, with corresponding boundary classical or double forces interpreted as reaction forces.

The virtual displacement field is assumed as simply as possible, with the virtual strain gradient, on which the double stress $\mu_{kji}^s = \mu_{kij}^s$ performs work, given as the double derivative $\delta u_{i,jk}^d$ regardless of material properties.

Integration by parts of the terms at the left-hand side of Eq. (13) and application of the divergence theorem leads to

$$
\begin{aligned}
&-\int_\Omega \left(\sigma_{ji,j}^s + f_i\right)\delta u_i^d \mathrm{d}\Omega + \int_\Gamma \left(\sigma_{ji}^s n_j - P_i\right)\delta u_i^d \mathrm{d}\Gamma \\
&+\int_\Gamma \mu_{kji}^s n_k \delta u_{i,j}^d \mathrm{d}\Gamma - \int_\Gamma Q_{is}\delta u_{i,s}^d \mathrm{d}\Gamma - \int_\Gamma R_i \delta q_i^d \mathrm{d}\Gamma = 0
\end{aligned}
\tag{15}
$$

The first two integral terms on the left are already expressed by means of the total stress σ_{ji}^s, defined in Eq. (4) – similarly to the classical elasticity theory. The domain integral is void, according to Eq. (5). Modifying the third integral term, according to the identity of Eq. (3), one obtains from Eq. (15)

$$
\begin{aligned}
&\int_\Gamma \left(\sigma_{ji}^s n_j - P_i\right)\delta u_i^d \mathrm{d}\Gamma + \int_\Gamma \left(\mu_{kji}^s n_k n_j n_l \delta u_{i,l}^d - R_i \delta q_i^d\right)\mathrm{d}\Gamma \\
&+\int_\Gamma \left(\mu_{kji}^s n_k \left(\delta_{jl} - n_j n_l\right)\delta u_{i,l}^d - Q_{is}\delta u_{i,s}^d\right)\mathrm{d}\Gamma = 0
\end{aligned}
\tag{16}
$$

or, substituting δq_i^d for $n_l \delta u_{i,l}^d$, according to Mindlin's proposition that the variation of the normal gradient on Γ should be independent from the displacement variation,

$$
\begin{aligned}
&\int_\Gamma \left(\sigma_{ji}^s n_j - P_i\right)\delta u_i^d \mathrm{d}\Gamma + \int_\Gamma \left(\mu_{kji}^s n_k n_j - R_i\right)\delta q_i^d \mathrm{d}\Gamma \\
&+\int_\Gamma \left(\mu_{kji}^s n_k \left(\delta_{jl} - n_j n_l\right)\delta u_{i,l}^d - Q_{is}\delta u_{i,s}^d\right)\mathrm{d}\Gamma = 0
\end{aligned}
\tag{17}
$$

[1] There is some confusion in the literature on the denomination of T_{ij} and R_i, as both are usually referred to as *double tractions*. In this paper, the qualificative *normal* is used for the latter. The static action referred to by Mindlin as T_{ji} is not used in the subsequent developments. In general, the notation proposed by Mindlin (1964) is followed as closely as possible, with the only flagrant exception that lower case is used for the body forces f_i in order to be consistent with previous developments in the classical elasticity. Moreover, one resorts to the *tangential* double tractions Q_{is} proposed by Mindlin, which perform virtual work on tangential displacement gradients $\delta u_{i,s}^d$, although in a way that is apparently inedited in the technical literature.

This is a natural assumption in the frame of a hybrid variational formulation, and consistent with the boundary-only integral statement just obtained. In fact, u_i^d is defined only on Γ, according to Eq. (12), in terms of boundary parametric variables, with $u_{in} \equiv u_{in}(\xi)$ for 2D problems or $u_{in} \equiv u_{in}(\xi,\eta)$ for 3D problems. There is no possibility of defining how u_i^d varies across the boundary, except by explicitly introducing an independent field q_i^d, as done in Eq. (12).

Mindlin (1964), followed by other researchers, proposed a manipulation of the integral that contains the term $\left(\delta_{jl} - n_j n_l\right)$ in Eq. (17) in order to enable the implementation of a numerical model. This ends up requiring the computation of "jumping" terms, for a non-smooth boundary of a 3D problem. Moreover, it introduces the need of special static boundary conditions related to the jumping terms. Remarkably, several authors show numerical implementations that have become feasible only by artificially smoothing the boundary around corner points. Three-dimensional implementations seem to be extremely complicated in such a framework [Amanatidou and Aravas (2002); Polyzos, Tsepoura, Tsinopoulos, and Beskos (2003)]. However, Mindlin's proposition is naturally circumvented in the present outline. Firstly, one recognizes that the term $\left(\delta_{jl} - n_j n_l\right)$ in Eq. (17) is orthogonally projecting $\delta u_{i,l}^d$ onto the tangent plane to Γ at a given point ξ, for 2D problems, or (ξ,η), for 3D problems. As a result, only the projection $\delta q_i^d = n_l \delta u_{i,l}^d$ of $\delta u_{i,l}^d$ onto the normal to Γ requires an independent discretization, which is done according to Eq. (12).

Two-dimensional numerical models may be formulated from Eq. (17) directly as

$$\int_\Gamma \left(\sigma_{ji}^s n_j - P_i\right)\delta u_i^d \mathrm{d}\Gamma + \int_\Gamma \left(\mu_{kji}^s n_k n_j - R_i\right)\delta q_i^d \mathrm{d}\Gamma + \int_\Gamma \left(\mu_{kji}^s n_k |J|^{-2} t_j - Q_{i\xi}\right)\delta u_{i,\xi}^d \mathrm{d}\Gamma = 0 \tag{18}$$

where $\delta u_{i,\xi}^d \equiv \delta \mathrm{d}u_i^d/\mathrm{d}\xi = u'_{in}\delta d_n$ on Γ comes from $t_l \delta u_{i,l}^d \equiv \delta \mathrm{d}u_i^d/\mathrm{d}\xi$ and $\delta_{jl} - n_j n_l = |J|^{-2} t_j t_l$, in which one defines the tangent vector $\mathbf{t} = [\mathrm{d}x/\mathrm{d}\xi \quad \mathrm{d}y/\mathrm{d}\xi]^{\mathrm{T}}$ and the Jacobian $|J| \equiv |\mathbf{t}|$, always making use of Eq. (12). Of course, no sum is meant by the repetition of ξ in the last term of the above equation.

Three-dimensional numerical models are also formulated directly from Eq. (17) as

$$\int_\Gamma \left(\sigma_{ji}^s n_j - P_i\right)\delta u_i^d \mathrm{d}\Gamma + \int_\Gamma \left(\mu_{kji}^s n_k n_j - R_i\right)\delta q_i^d \mathrm{d}\Gamma + \int_\Gamma \left(\mu_{kji}^s n_k |J|^{-2} \tilde{t}_{js} - Q_{is}\right)\delta u_{i,s}^d \mathrm{d}\Gamma = 0 \tag{19}$$

To arrive at this equation, one firstly defines the tangent vectors in terms of $u_{in} \equiv$

$u_{in}(\xi,\eta)$ in Eq. (12):

$$\mathbf{u} = [\partial x/\partial\xi \quad \partial y/\partial\xi \quad \partial z/\partial\xi]^{\mathrm{T}} \tag{20}$$

$$\mathbf{v} = [\partial x/\partial\eta \quad \partial y/\partial\eta \quad \partial z/\partial\eta]^{\mathrm{T}} \tag{21}$$

For $|J|^2 = |\mathbf{u}\times\mathbf{v}|$ and defining the matrices $\mathbf{t} = [\mathbf{u} \quad \mathbf{v}]$ and $\mathbf{t}^{\perp} = [\mathbf{v} \quad -\mathbf{u}]$, one obtains that

$$\delta_{jl} - n_j n_l = |J|^{-2} t_{jr} t^{\perp}_{mr} t^{\perp}_{ms} t_{ls} \tag{22}$$

The indices r and s vary from 1 to 2, as they refer to ξ and η. One identifies in Eq. (19) that $\delta u^d_{i,s}$ comes from $t_{ls}\delta u^d_{i,l} \equiv \delta u^d_{i,s}$, where $()_{,s}$ denotes derivatives with respect to ξ and η. According to Eq. (22), $\tilde{t}_{js} = t_{jr} t^{\perp}_{mr} t^{\perp}_{ms}$. [2]

Taking Eq. (18), for 2D problems, as just a particular case of Eq. (19), in terms of notation, one writes the numerical expression of the virtual work principle of Eq. (13), for stresses and displacements approximated according to Eqs. (8,9,10, 11, 12), as:

$$\langle \delta d_n \quad \delta q_\ell \rangle \left(\begin{bmatrix} \int_\Gamma \left(\sigma^*_{jim} n_j u_{in} + \mu^*_{kjim} n_k |J|^{-2} \tilde{t}_{js} u_{in,s} \right) \mathrm{d}\Gamma \\ \int_\Gamma \mu^*_{kjim} n_k n_j q_{i\ell} \mathrm{d}\Gamma \end{bmatrix} \{p^*_m\} \right. \tag{23}$$

$$\left. + \begin{Bmatrix} \int_\Gamma \left(\sigma^p_{ji} n_j u_{in} + \mu^p_{kji} n_k |J|^{-2} \tilde{t}_{js} u_{in,s} \right) \mathrm{d}\Gamma \\ \int_\Gamma \mu^p_{kji} n_k n_j q_{i\ell} \mathrm{d}\Gamma \end{Bmatrix} - \begin{Bmatrix} \int_\Gamma (P_i u_{in} + Q_{is} u_{in,s}) \mathrm{d}\Gamma \\ \int_\Gamma R_i q_{i\ell} \mathrm{d}\Gamma \end{Bmatrix} \right) = 0$$

Since this equation holds for arbitrary δd_n and δq_ℓ, one obtains the matrix equilibrium system

$$\mathbf{H}^{\mathrm{T}} \mathbf{p}^* = \mathbf{p} - \mathbf{p}^p \tag{24}$$

in which the equilibrium matrix $\mathbf{H}^{\mathrm{T}}$ as well as the vectors of nodal forces $\mathbf{p}$ and $\mathbf{p}^p$, which are equivalent to the boundary and domain traction forces, respectively, are inferred from Eq. (23). A detailed discussion of Eq. (24) is carried out in the next sections. One obtains from this equation the formal relation of the tangential double

[2] It is possible to arrive at simpler expressions of Eqs. (18) and (19) by using normalized expressions of $\mathbf{t}$ as well as by referring to the surface length in the definition of Q_{is} and $\delta u^d_{i,s}$, so that $|J|^{-2}$ drops out. However, the proposed expressions seem easier to grasp mechanically and more efficient in terms of code writing. In the three-dimensional model, $|J| \equiv |g|$, where $g_{rs} \equiv g_{\alpha\beta}$ is the surface metric tensor, according to the literature on differential geometry [Kreyszig (1991)]. The product $|J|^{-1} t^{\perp}_{mr} t^{\perp}_{ms}$ is the inverse of g_{rs}.

tractions Q_{is} with the double stress μ_{kji} on the boundary, as generally expressed for a 3D problem:

$$Q_{is} = \mu_{kji} n_k |J|^{-2} \tilde{t}_{js} \tag{25}$$

or, in the particular application based on Aifanti's proposition, according to Eq. (6) (without the subscript s in order to refer to a general stress field),

$$Q_{is} = g^2 \tau_{ji,k} n_k |J|^{-2} \tilde{t}_{js} \tag{26}$$

4.2 Stress virtual work for displacement compatibility checking

The second statement that comes from the Hellinger-Reissner potential may be obtained by weakly enforcing compatibility of the displacements u_i^s and u_i^d in terms of the stress virtual work equation

$$\int_\Omega \left(u_{i,j}^s - u_{i,j}^d\right) \delta\tau_{ji}^* \mathrm{d}\Omega + \int_\Omega \left(u_{i,jk}^s - u_{i,jk}^d\right) \delta\mu_{kji}^* \mathrm{d}\Omega = 0 \tag{27}$$

Integrating by parts the terms of this equation, applying the divergence theorem and using Eq. (4), one arrives at

$$-\int_\Omega \delta\sigma_{ji,j}^* \left(u_i^s - u_i^d\right) \mathrm{d}\Omega + \int_\Gamma \delta\sigma_{ji}^* n_j \left(u_i^s - u_i^d\right) \mathrm{d}\Gamma + \int_\Gamma \delta\mu_{kji}^* n_k \left(u_{i,j}^s - u_{i,j}^d\right) \mathrm{d}\Gamma = 0 \tag{28}$$

The domain integral of this equation is void, according to Eq. (5). As done in the preceding Section, one splits the displacement gradient into normal and tangential contributions, thus obtaining, in the notation for 3D problems ,

$$\begin{aligned} &\int_\Gamma \delta\sigma_{ji}^* n_j \left(u_i^s - u_i^d\right) \mathrm{d}\Gamma + \int_\Gamma \delta\mu_{kji}^* n_k u_{i,j}^s \mathrm{d}\Gamma \\ &- \int_\Gamma \delta\mu_{kji}^* n_k n_j q_i^d \mathrm{d}\Gamma - \int_\Gamma \delta\mu_{kji}^* n_k |J|^{-2} \tilde{t}_{js} u_{i,s}^d \mathrm{d}\Gamma = 0 \end{aligned} \tag{29}$$

In this equation, one states that the boundary displacement gradient q_i^d is described independently from the displacement u_i^d. This is a step forward from the assumption made explicit in the statement before Eq. (17) and with reference to Mindlin, which refers to the independence of variations. The assumption embedded in the above equation is in consonance with the proposition made by Polyzos, Tsepoura, Tsinopoulos, and Beskos (2003) in the frame of the collocation boundary element method. Introducing the approximations for stresses and displacements given in Eqs. (8 – 12), one writes the numerical expression of the virtual work principle of

Eq. (27) as

$$\langle \delta p_m^* \rangle \left(\left[\int_\Gamma \left(\sigma_{jim}^* n_j u_{in}^* + \mu_{kjim}^* n_k u_{in,j}^* \right) \mathrm{d}\Gamma + \int_\Gamma \left(\sigma_{jim}^* n_j u_{is}^r + \mu_{kjim}^* n_k u_{is,j}^r \right) \mathrm{d}\Gamma C_{sn} \right] \{p_n^*\} \right.$$
$$- \left[\int_\Gamma \left(\sigma_{jim}^* n_j u_{in} + \mu_{kjim}^* n_k |J|^{-2} \tilde{t}_{js} u_{in,s} \right) \mathrm{d}\Gamma \quad \int_\Gamma \mu_{kjim}^* n_k n_j q_{i\ell} \mathrm{d}\Gamma \right] \left\{ \begin{array}{c} d_n \\ q_\ell \end{array} \right\}$$
$$\left. + \left\{ \int_\Gamma \left(\sigma_{jim}^* n_j u_i^p + \mu_{kjim}^* n_k u_{i,j}^p \right) \mathrm{d}\Gamma \right\} \right) = 0 \tag{30}$$

Since δp_m^* is arbitrary, one obtains the matrix compatibility system

$$\mathbf{F}^* \mathbf{p}^* = \mathbf{H}\mathbf{d} - \mathbf{b} \tag{31}$$

4.3 A first assessment of the matrices from the Hellinger-Reissner potential

The expressions of the flexibility matrix $\mathbf{F}^*$ and of the kinematic transformation matrix $\mathbf{H}$ for the finite element implementation are:

$$\mathbf{F}^* = \left[\int_\Gamma \left(\sigma_{jim}^* n_j u_{in}^* + \mu_{kjim}^* n_k u_{in,j}^* \right) \mathrm{d}\Gamma \right] \tag{32}$$

since the term multiplying C_{sn} in Eq. (30) is void by definition, and

$$\mathbf{H} = \left[\begin{array}{cc} \int_\Gamma \left(\sigma_{jim}^* n_j u_{in} + \mu_{kjim}^* n_k |J|^{-2} \tilde{t}_{js} u_{in,s} \right) \mathrm{d}\Gamma & \int_\Gamma \mu_{kjim}^* n_k n_j q_{i\ell} \mathrm{d}\Gamma \end{array} \right] \tag{33}$$

Moreover, the vector $\mathbf{p}$ of equivalent nodal forces, for applied boundary tractions, is, according to Eqs. (23) and (24),

$$\mathbf{p} = \left\{ \begin{array}{c} \int_\Gamma (P_i u_{in} + Q_{is} u_{in,s}) \mathrm{d}\Gamma \\ \int_\Gamma R_i q_{i\ell} \mathrm{d}\Gamma \end{array} \right\} \tag{34}$$

Finally, the vectors of equivalent nodal forces $\mathbf{p}^p$ and equivalent nodal displacements $\mathbf{b}$, for body forces (or any particular solution of the problem's differential equation one may know in advance) are obtained from Eqs. (23) and (30):

$$\mathbf{p}^p = \left\{ \begin{array}{c} \int_\Gamma \left(\sigma_{ji}^p n_j u_{in} + \mu_{kji}^p n_k |J|^{-2} \tilde{t}_{js} u_{in,s} \right) \mathrm{d}\Gamma \\ \int_\Gamma \mu_{kji}^p n_k n_j q_{i\ell} \mathrm{d}\Gamma \end{array} \right\} \tag{35}$$

$$\mathbf{b} = \left\{ \int_\Gamma \left(\sigma_{jim}^* n_j u_i^p + \mu_{kjim}^* n_k u_{i,j}^p \right) \mathrm{d}\Gamma \right\} \tag{36}$$

4.4 Stiffness matrix of the finite/boundary element formulation

Solving for $\mathbf{p}^*$ in Eq. (31) and substituting into Eq. (24), one obtains the nodal equilibrium equation

$$\mathbf{H}^{\mathrm{T}}\mathbf{F}^{*(-1)}\mathbf{H}\mathbf{d} = \mathbf{p} - \mathbf{p}^p + \mathbf{H}^{\mathrm{T}}\mathbf{F}^{*(-1)}\mathbf{b} \tag{37}$$

In this equation, one recognizes that a stiffness matrix

$$\mathbf{K} = \mathbf{H}^{\mathrm{T}}\mathbf{F}^{*(-1)}\mathbf{H} \tag{38}$$

has been naturally arrived at. The terms on the right in Eq. (37) account for the action of boundary and domain forces, according to the assumptions previously made. The vector $\mathbf{d}$ comprises both nodal displacements d_n and nodal normal gradients q_ℓ. The flexibility matrix $\mathbf{F}^*$ is symmetric by construction. For elastostatics problems, $\mathbf{F}^*$ is a singular matrix whether coming from a formulation with singular (boundary element) or non-singular (finite element) fundamental solutions. In fact, $\mathbf{F}^*$ and $\mathbf{H}$ feature the same spectral properties of the classical elasticity formulation [Dumont (2003); Dumont and Huamán (2009)], in which respects the nodal displacements d_n of Eq. (30), which are accompanied by sets of the normal gradients q_ℓ related to rigid body rotations. This is numerically illustrated in Section 5 and explained in detail in Section 6. In the finite element implementation of Eq. (37), one constructs the kinematic matrix $\mathbf{H}$ of Eqs. (23, 24) with n^* rows and n^d columns and rank equal to $n^d - n^{rig}$, where n^{rig} is the number of columns of $\mathbf{W} = N(\mathbf{H}^{\mathrm{T}}\mathbf{H})$ that span the space of rigid body displacements. One also constructs the flexibility matrix $\mathbf{F}^*$ of Eqs. (30, 31) of order n^* and rank $n^* - n^{rig}$, where $\mathbf{V} = N(\mathbf{F}^*)$ is a matrix with n^{rig} columns. For homogeneous materials and non-singular fundamental solutions, the generalized boundary displacements u_i^d and q_i^d of Eq. (12) are linear combinations of u_{im}^* in Eq. (10), and $\mathbf{V} = N(\mathbf{F}^*) \Rightarrow \mathbf{H}^{\mathrm{T}}\mathbf{V} = \mathbf{0}$. As already developed in the frame of the hybrid finite/boundary element method [Dumont (2003); Dumont and Prazeres (2005); Dumont and Aguilar (2009)], the generalized inversion of $\mathbf{F}^*$ in Eq. (37) is carried out by simply replacing $\mathbf{F}^{*(-1)}$ with $\left(\mathbf{F}^* + \mathbf{V}\mathbf{V}^{\mathrm{T}}\right)^{-1}$.

For non-singular fundamental solutions, $\mathbf{H}$ is usually a rectangular matrix, as, for the adequate representation of the deformed state in the domain, the dimension of $\mathbf{p}^*$ must be at least equal to the dimension of $\mathbf{d}$ added with the dimension of $\mathbf{q}$ [Dumont and Huamán (2009); Huamán (2013)]. As shown in Table 1, $\mathbf{H}$ is a square matrix only for the 3D, eight-node brick element H8, besides the trivial cases of truss and beam elements (which topologically fit into the case of singular fundamental solutions [Dumont and Huamán (2009); Huamán (2013)]).

5 Application to truss and beam elements

5.1 Truss element

The homogeneous differential equation of a truss element of length L, constant cross section A and elasticity modulus E is

$$\frac{\mathrm{d}^2u^*}{\mathrm{d}x^2} - g^2\frac{\mathrm{d}^4u^*}{\mathrm{d}x^4} = 0, \quad \text{with solutions} \quad \mathbf{u}^* = \left\langle e^{x/g} \;\; e^{-x/g} \;\; x \;\; 1 \right\rangle \tag{39}$$

As outlined by Dumont and Huamán (2009), the corresponding stiffness matrix, for the degrees of freedom given in the first scheme of Fig. 1 and substituting $\bar{g}$, C and S for g/L, $\cosh(L/g)$ and $\sinh(L/g)$, is

$$\mathbf{K} = \frac{EA/L}{S + 2\bar{g} - 2C\bar{g}} \begin{bmatrix} S & g(C-1) & -S & g(C-1) \\ g(C-1) & gL(C - S\,\bar{g}) & g(1-C) & gL(S\,\bar{g}-1) \\ -S & g(1-C) & S & g(1-C) \\ g(C-1) & gL(S\,\bar{g}-1) & g(1-C) & gL(C - S\,\bar{g}) \end{bmatrix} \tag{40}$$

The null space of this stiffness matrix is the vector of rigid body displacements $\mathbf{W} = \langle 1 \;\; 0 \;\; 1 \;\; 0 \rangle^{\mathrm{T}}$. One checks that a constant strain state given by the vector of displacements $\langle -1/2 \;\; 1/L \;\; 1/2 \;\; 1/L \rangle$ yields only classical forces $\frac{EA}{L}\langle -1 \;\; 0 \;\; 1 \;\; 0 \rangle$ as a response (which also clarifies the meaning of the non-classical displacement degrees of freedom in terms of the global coordinates schematically represented in Fig. 1). Moreover, if one assembles the stiffness matrices of two elements of lengths αL and $(1-\alpha)L$, for any $0 \le \alpha \le 1$, and performs static condensation of the internal degrees of freedom, the above stiffness matrix $\mathbf{K}$ is retrieved.

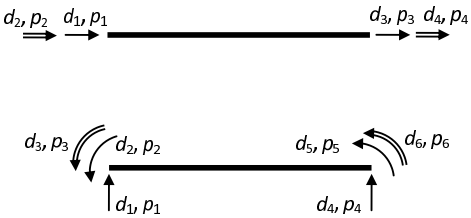

Figure 1: Schematic representation of the generalized, globally oriented, displacement and force degrees of freedom of truss and beam elements.

5.2 Slender beam element

The application of the Euler-Bernoulli hypothesis to thin beams, plates and shells in the frame of the strain gradient elasticity is an oxymoron, to say the least. An

attempt to consistently assess general bending problems in the present framework is in progress. Nevertheless, it may be academically worth applying the present developments to a slender beam, which has already been the subject of many research works [Challamel and Wang (2008); Papargyri-Beskou and Beskos (2008, 2009); Papargyri-Beskou, Polyzos, and Beskos (2009); Reddy (2007); Kahrobaiyan, Asghari, Rhaeifard, and Ahmadian (2011)]. The homogeneous differential equation is

$$\frac{\mathrm{d}^4 u^*}{\mathrm{d}x^4} - g^2 \frac{\mathrm{d}^6 u^*}{\mathrm{d}x^6} = 0, \quad \text{with solutions} \quad \mathbf{u}^* = \left\langle g^4 e^{x/g} \;\; g^4 e^{-x/g} \;\; x^3 \;\; x^2 \;\; x \;\; 1 \right\rangle \tag{41}$$

For a constant moment of inertia I, the corresponding stiffness matrix is

$$\mathbf{K} = \begin{bmatrix} K_{11} & K_{11}L/2 & K_{13} & -K_{11} & K_{11}L/2 & -K_{13} \\ sym & K_{22} & K_{23} & -K_{11}L/2 & K_{11}L^2/2 - K_{22} & K_{23} - K_{13}L \\ sym & sym & K_{33} & -K_{13} & K_{13}L - K_{23} & -K_{36} \\ sym & sym & sym & K_{11} & -K_{11}L/2 & K_{13} \\ sym & sym & sym & sym & K_{22} & -K_{23} \\ sym & sym & sym & sym & sym & K_{33} \end{bmatrix} \tag{42}$$

where

$$\begin{aligned} K_{11} &= 12(2C - 2 - S/\bar{g})\Delta, \qquad K_{22} = 4L^2(3C - 3S\bar{g} - S/\bar{g})\Delta, \\ K_{33} &= L^4\left(4S\bar{g} - C - 24(S - C\bar{g} + \bar{g})\bar{g}^3 + 12\bar{g}^2\right)\Delta, \\ K_{13} &= 6L^2\left(4(1-C)\bar{g}^2 + 4S\bar{g} - 1 - C\right)\Delta, \\ K_{23} &= 2L^3\left(12(1-C)\bar{g}^2 - 1 + 9S\bar{g} - 2C\right)\Delta, \\ K_{36} &= L^4\left(2S\bar{g} + 1 + 24(S - C\bar{g} + \bar{g})\bar{g}^3 - 12C\bar{g}^2\right)\Delta \end{aligned} \tag{43}$$

with $\Delta = (8C + 24\bar{g}(C\bar{g} - S - \bar{g}) - S/\bar{g} + 4)\,EI/L^3$, for $\bar{g}$, C and S as before. This matrix has rank four and its null space is spanned by the vectors of rigid body displacements $\langle 1 \;\; 0 \;\; 0 \;\; 1 \;\; 0 \;\; 0 \rangle$ and $\langle 0 \;\; 1 \;\; 0 \;\; L \;\; 1 \;\; 0 \rangle$. Resorting to the second scheme of Fig. 1 for the global orientation of the degrees of freedom, one checks that classical pure bending $\frac{EI}{L}\langle 0 \;\; -1 \;\; 0 \;\; 0 \;\; 1 \;\; 0 \rangle$ is obtained from the vector of constant curvature $\langle 0 \;\; -1/2 \;\; 1/L \;\; 0 \;\; 1/2 \;\; 1/L \rangle$. Moreover, if one assembles the stiffness matrices of two elements of lengths αL and $(1-\alpha)L$, for any $0 \le \alpha \le 1$, and performs static condensation of the internal degrees of freedom, the above stiffness matrix $\mathbf{K}$ is also retrieved.

6 Conceptual assessments of 2D and 3D problems

6.1 Basic formulation

The homogeneous differential equation to be solved is [Polyzos, Tsepoura, Tsinopoulos, and Beskos (2003); Huamán (2013)]

$$\left(1-g^2\nabla\right)\left(u^*_{im,kk}+\frac{1}{1-2\nu}u^*_{km,ki}\right)=0 \tag{44}$$

Expressing u^*_{im} in terms of a potential function, $u^*_{im}=\delta_{im}\Phi_{0,kk}-\Phi_{0,im}/(2-2\nu)$, one arrives at the basic differential equation $(1-g^2\nabla^2)(\nabla^4\Phi_0)=0$, which must provide n^* solutions. The subscript of Φ_0 is justified because a general solution Φ for time-dependent problems in the frequency domain can be easily obtained. The solution of Φ_0 for 2D problems is expressed in polar coordinates (r,θ) as

$$\Phi_0=r^n\left[C_{1n}\cos(n\theta)+C_{2n}\sin(n\theta)\right]+I_n(r/g)\left[C_{3n}\cos(n\theta)+C_{4n}\sin(n\theta)\right] \tag{45}$$

where $I_n(r/g)$ is the modified Bessel function of the first kind and order n, with argument (r/g). The trigonometric terms in θ correspond to $n^*=4(2n+1)$ complete polynomials or order n, rigid body displacements included. For 3D problems, the solution is expressed in spherical coordinates (r,θ,ϕ) as

$$\begin{aligned}\Phi_0=P^n_\ell(\cos\theta)\Big\{r^n\Big[(r^2+4n+6)g^2+4n\Big])\left[C_{1\ell}\cos(\ell\phi)+C_{2\ell}\sin(\ell\phi)\right]\\ +I_{\frac{1}{2}+n}(r/g)\left[C_{3\ell}\cos(\ell\phi)+C_{4\ell}\sin(\ell\phi)\right]/\sqrt{r}\Big\}\end{aligned} \tag{46}$$

where the Bessel function $I_{\frac{1}{2}+n}(r/g)$ of fractional order is actually a polynomial and $P^n_\ell(\cos\theta)$ is the associated Legendre function of first kind, degree n and order ℓ with argument $(\cos\theta)$, also a polynomial in Cartesian coordinates. $P^n_\ell(\cos\theta)$ exists only for $\ell\le n$. There are $4n+2$ solutions in Eq. (46), with a total of $n^*=6(n+1)^2$ solutions u^*_{im} comprised by a complete polynomial of degree n, rigid body displacements included.

6.2 Finite element implementation and results

To make sure that the formulation is always well posed and the final expression of the stiffness matrix **K** in Eq. (38) is independent from the location of the finite element in the Cartesian coordinate frame, the number n^* of internal parameters must correspond to a complete polynomial, whose order n is chosen in such a way that $n^*\ge n^d$. Table 1 illustrates the results for some common finite element patterns (one obtains $n^*=n^d$ only for CST and Te4 elements in classical elasticity [Dumont and Prazeres (2005)], but this also happens for the H8 element shown in the Table).

Since the evaluation of $\mathbf{H}$ and $\mathbf{F}^*$ is carried out only in terms of boundary integrals, according to Eqs. (23) and (30), one may construct finite elements of any shape, provided that n^* is not too large, as ill-conditioning will certainly arise (differently from which occurs in a boundary element formulation based on singular fundamental solutions). Figure 2 illustrates the assemblage of three quadrilateral elements

Table 1: Illustration of the number n^* of solutions necessary for the implementation of some 2D and 3D finite elements (CST, T6 = 3, 6 node triangles; Q4, Q8 = 4, 8 node quadrilaterals; Te4, Te10 = 4, 10 node tetrahedrons; H8, H20 = 8, 20 node hexahedrons).

	2D problems				3D problems			
Polynomial order n	2	3	4	5	2	3	4	5
n^* internal degrees of freedom	$4(2n+1)$				$6(n+1)^2$			
	20	28	36	42	54	96	150	216
Element type	CST	Q4	T6	Q8	Te4	H8	Te10	H20
n^d external d.o.f.	18	24	30	40	48	96	102	204

with linear boundary interpolation functions for u_i^d and q_i^d (Q4). Two classical degrees of freedom are represented at each node (numbered from 1 to 14). Pairs of non-classical, globally oriented, degrees of freedom are also schematically represented at each edge extremity (in the drawing, they are shown at a small distance from the extremities only to characterize to which edge they actually correspond). While the classical degrees of freedom are nodal attributes, the non-classical ones are either edge or face attributes, for 2D or 3D elements. This accounts for the huge number of extra degrees of freedom that must be taken into account in a finite element implementation, as illustrated in Table 1 and in the Figure. As already mentioned for the truss and beam elements, the non-classical degrees of freedom, for the stiffness matrix obtained as in Eq. (37), are negatively oriented at negative faces or edges. Since one can tell that the left edges of the truss and beam elements are the negative ones, for the schemes of Fig. 1, the expressions of $\mathbf{K}$ in Eqs. (40) and (42) already take this fact into account, so that elements can be assembled in a straightforward way. For general 2D and 3D finite elements, however, which can be of any shape and orientation, one must always decide which edges or faces are negative (in terms of their outward normals) and multiply the corresponding rows and columns of the non-classical degrees of freedom by (-1) before assemblage. Such a need of reversing orientation was already mentioned by Mindlin (1964), although not in the context of a finite element implementation.

The matrix $\mathbf{W}$ of rigid body displacements, as introduced in the paragraph after Eq. (38), depends only on the structure's geometry. The vector of rigid body

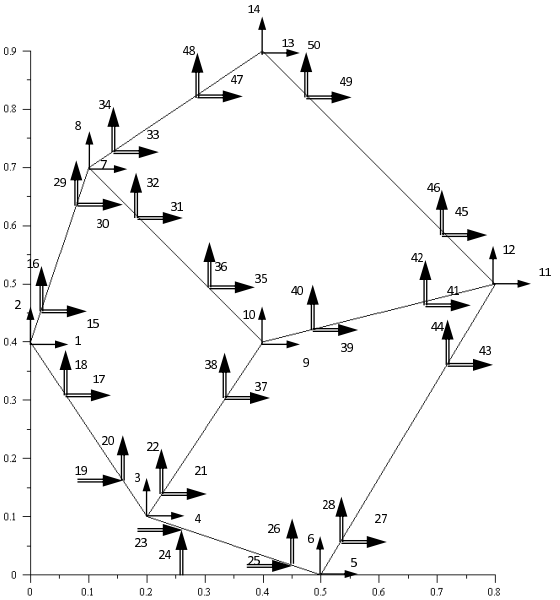

Figure 2: Assemblage of three quadrilateral elements with linear boundary interpolation functions.

rotations include coefficients of the normal gradient displacements q_ℓ that render only tangential components, which means that their normal projections, as defined in Eq. (3), are void in such a case. The matrix $\mathbf{V}$, required in the inversion of $\mathbf{F}^*$, can be constructed directly from the fundamental solutions derived from the potential functions of Eqs. (45) and (46), independently from geometry [Huamán (2013)]. They are arranged as

$$\mathbf{W} = \begin{bmatrix} \mathbf{W}_d \\ \mathbf{W}_q \end{bmatrix}, \qquad \mathbf{V} = \begin{bmatrix} \mathbf{V}_d \\ \mathbf{V}_q \equiv \mathbf{0} \end{bmatrix} \tag{47}$$

Both matrices $\mathbf{W}_d$ and $\mathbf{V}_d$ coincide with the ones obtained for the classical elasticity developments, as given by Dumont and Prazeres (2005) for 2D and 3D problems. The submatrices $\mathbf{W}_d$ and $\mathbf{W}_q$ of rigid body displacements are straightforward to construct, as given below (not normalized), with the subscripts n and ℓ referring exceptionally to classical and non-classical nodes (and not to degrees of freedom, as in the rest of the paper) for a discrete model with nodal points of coordinates either (x_n, y_n) or (x_n, y_n, z_n) and outward normal components (n_{x_ℓ}, n_{y_ℓ}) or $(n_{x_\ell}, n_{y_\ell}, n_{z_\ell})$:

$$\mathbf{W}_{d_n} = \begin{bmatrix} 1 & 0 & y_n \\ 0 & 1 & -x_n \end{bmatrix}, \quad \mathbf{W}_{q_\ell} = \begin{bmatrix} 0 & 0 & n_{y_\ell} \\ 0 & 0 & -n_{x_\ell} \end{bmatrix}, \quad \text{2D} \tag{48}$$

$$\mathbf{W}_{d_n} = \begin{bmatrix} 1 & 0 & 0 \\ 0 & 1 & 0 \\ 0 & 0 & 1 \\ 0 & -z_n & y_n \\ z_n & 0 & -x_n \\ -y_n & x_n & 0 \end{bmatrix}^{\mathbf{T}}, \quad \mathbf{W}_{q_\ell} = \begin{bmatrix} 0 & 0 & 0 \\ 0 & 0 & 0 \\ 0 & 0 & 0 \\ 0 & -n_{z_\ell} & n_{y_\ell} \\ n_{z_\ell} & 0 & -n_{x_\ell} \\ -n_{y_\ell} & n_{x_\ell} & 0 \end{bmatrix}^{\mathbf{T}}, \quad \text{3D} \tag{49}$$

As shown, the coefficients of $\mathbf{W}$ span all degrees of freedom of a model. Since $\mathbf{V} = N(\mathbf{F}^*)$, its non-zero coefficients affect only four of the simplest solutions for 2D problems or nine of the simplest solutions for 3D problems, Eqs. (45) and (46), as given below in non-normalized format [Dumont and Prazeres (2005); Huamán (2013)]:

$$\mathbf{V}_d = \begin{bmatrix} 1 & 0 & 0 & 0 & 0 & 0 & \cdots & 0 \\ 0 & 1 & 0 & 0 & 0 & 0 & \cdots & 0 \\ 0 & 0 & 0 & 1 & -1 & 0 & \cdots & 0 \end{bmatrix}^{\mathbf{T}}, \quad \text{2D} \tag{50}$$

$$\mathbf{V}_d = \begin{bmatrix} 1 & 0 & 0 & 0 & 0 & 0 & 0 & 0 & 0 & 0 & 0 & 0 & \cdots & 0 \\ 0 & 1 & 0 & 0 & 0 & 0 & 0 & 0 & 0 & 0 & 0 & 0 & \cdots & 0 \\ 0 & 0 & 1 & 0 & 0 & 0 & 0 & 0 & 0 & 0 & 0 & 0 & \cdots & 0 \\ 0 & 0 & 0 & 0 & 0 & 0 & 0 & 0 & -1 & 0 & 1 & 0 & \cdots & 0 \\ 0 & 0 & 0 & 0 & 0 & 1 & 0 & 0 & 0 & -1 & 0 & 0 & \cdots & 0 \\ 0 & 0 & 0 & 0 & -1 & 0 & 1 & 0 & 0 & 0 & 0 & 0 & \cdots & 0 \end{bmatrix}^{\mathbf{T}}, \quad \text{3D} \tag{51}$$

The numerical code presently implemented applies to 2D finite elements of any shape and any number of straight or curved edges with linear, quadratic or cubic boundary interpolation functions. In Huamán (2013), a rectangular element was tested with the length increasingly larger than the hight. The coefficients of the stiffness matrix corresponding to longitudinal degrees of freedom tended to the coefficients of the stiffness matrix of a truss element of corresponding mechanical properties, Eq. (40), drawing the authors' attention to the fact that negative faces require reverse orientation of the non-classical degrees of freedom. A second run consisted in evaluating the stiffness matrices of several irregular quadrilaterals, as shown in Fig. 2, for a series of patch tests. Equivalent nodal forces $\mathbf{p}$ were evaluated according to Eqs. (23) and (24) for linear, quadratic and cubic fields comprised by the fundamental solutions u^*_{im}. Equation (31) was also checked for the corresponding nodal vectors $\mathbf{d}$ that comprise both displacements and normal gradients. For the linear field, complete agreement was achieved, also leading to only classical forces, as required. The quadratic and cubic fields are not exactly represented by the Q8 elements. However, the assemblage of the elements led to zero forces for classical and non-classical resultants along the edges between two elements, and particularly

at the node that joins all three elements in Fig. 2, which is a strict consistency check of the whole formulation.

According to the explanation after Eq. (46), the 3D non-singular solution of the homogeneous differential Eq. (44) is actually polynomial. The complete 2D solution, Eq. (45), involves the evaluation of modified Bessel functions of the first kind and order n, where n increases with the number of required solutions. However, this Bessel function also has a polynomial expansion, although convergence of the resulting series may become difficult to deal with for large arguments r/g. On the other hand, one obtains from Eq. (44) that a solution of the classical elasticity is also a solution of the present problem, only that the number of polynomial terms required in the matrix formulation of Section 4 may become very large, as shown in Table 1, with ensuing ill-conditioning. Numerical tests have been performed with both formulation possibilities of the problem – with and without the use of Bessel functions. The results have turned out similar, although the use of plain polynomial solutions – the first part of Eq. (45) – have become by far easier to deal numerically. Plain polynomial solutions have been consequently adopted in the ultimate numerical implementation of the developed matrices.

7 Two-dimensional finite element applications

7.1 A convergence test for linear quadrilateral elements

A convergence test is carried out for a parallelogram-shaped elastic body modeled with either 2×2, 4×4 (illustrated in Fig. 3), 8×8, 12×12 or 16×16 linear quadrilateral elements (elements Q4 of Table 1). Since each finite element node has 6 degrees of freedom (dof), the proposed meshes correspond to either 66, 210, 738, 1586 or 2754 dof, respectively. The mechanical properties are, in consistent units, $G = 10^5$, $\nu = 0.2$ and g equal to either 0, 0.1, 0.2 or 0.3.

A cubic displacement field (the subscript stands for *polynomial*),

$$u_i^p = \begin{Bmatrix} 3x^3 - 8x^3\nu - 21xy^2 + 24xy^2\nu \\ 3(x^2+y^2)y \end{Bmatrix} \tag{52}$$

which satisfies Eq. (44), is applied to the elastic body, with corresponding classical traction forces P_i as well as double tangential and normal forces Q_i and R_i, defined in Section 4.1, given as

$$P_i{}^p = 6G \begin{Bmatrix} (3-4\nu)n_1x^2 - 2(3-4\nu)n_2xy + (4\nu-7)n_1y^2 + 8n_1g^2 \\ (1+4\nu)n_2x^2 - 2(3-4\nu)n_1xy + (3-4\nu)n_2y^2 - 8n_2g^2 \end{Bmatrix} \tag{53}$$

$$Q_i^p = \frac{12G}{J^2} \begin{Bmatrix} (3-4\nu)(n_1t_1 - n_2t_2)xg^2 + (-(3-4\nu)n_1t_2 - (7-4\nu)n_2t_1)yg^2 \\ ((1+4\nu)n_1t_2 - (3-4\nu)n_2t_1)xg^2 + (3-4\nu)(-n_1t_1 + n_2t_2)yg^2 \end{Bmatrix} \tag{54}$$

$$R_i{}^p = 12G \begin{Bmatrix} (3-4\nu)xg^2(n_1^2-n_2^2) - 2(5-4\nu)yg^2 n_1 n_2 \\ -2(1-4\nu)xg^2 n_1 n_2 - (3-4\nu)yg^2(n_1^2-n_2^2) \end{Bmatrix} \tag{55}$$

In these equations, n_i are the components of the outward unit normal to the boundary, and t_i are the tangent components, with J representing the Jacobian of the boundary parametric transformation, as introduced before. Two other polynomial fields, of fourth and fifth degrees, are also applied:

$$u_i{}^p = \begin{Bmatrix} -x^4(1-4\nu) + x^2y^2(18-24\nu) - y^4(5-4\nu) \\ -4xy(x^2+y^2) \end{Bmatrix} \tag{56}$$

$$u_i{}^p = \begin{Bmatrix} 15x^5 - 30x^3y^2 - 45xy^4 \\ 3y(-5x^4(9-8\nu) + 10x^2y^2(5-8\nu) - y^4(1-8\nu) \end{Bmatrix} \tag{57}$$

The corresponding boundary forces are not shown, for space restriction, but can be easily evaluated [Huamán (2014)].

7.1.1 Convergence tests for nodal force equilibrium in the domain

In order to estimate the magnitude of the errors one should expect in the numerical calculations, the errors in the evaluation of classical nodal forces at the center node of the parallelogram, for $g = 0$, is shown on the right of Fig. 3, according to the norm

$$error(p_i) = \frac{\left|K_{ij}d_j\right|}{\left|K_{ij}\right|\left|d_j\right|} \tag{58}$$

where **K** is the stiffness matrix defined in Eq. (38) and **d** are nodal displacements and gradient displacements corresponding to the applied polynomial fields. This error should be equal to zero, since there are no applied domain forces inside the parallelogram. "Classical nodal forces" **P** actually represent the upper subvector of the equivalent nodal forces **p** of Eq. (34), which depend of g, as illustrated in Eqs. (53) and (54). Figure 3 show results only for the quartic and quintic polynomials. Results for applied cubic displacements are by far more accurate.

The same error estimates in the evaluation of classical nodal forces are shown for for $g = 0.1$ and $g = 0.2$ on the left of Fig. 4 and on the right of Fig. 5. For the non-classical forces, Eq. (58) does not apply to an individual degree of freedom. In fact, such an equilibrium statement seems to apply only to the sum of concurring non-classical forces at a given node. Figures 4, 5 and 6 display the convergence results of such forces grouped for the horizontal edges (H) and inclined edges (V) adjacent to the center node of the parallelogram. Since the results converge separately to zero, their sums also converge to zero.

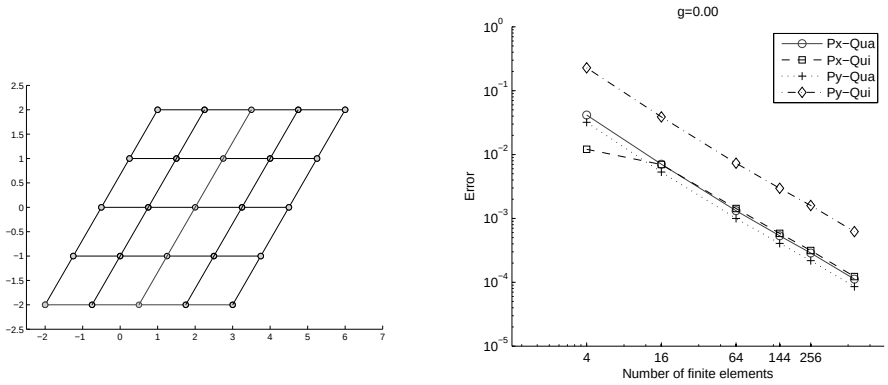

Figure 3: Left: Parallelogram-shaped elastic body modeled with either 4, 16, 64, 144 or 256 quadrilateral elements. Right: Error in the evaluation of classical nodal forces, for $g = 0$, at the center node of the parallelogram.

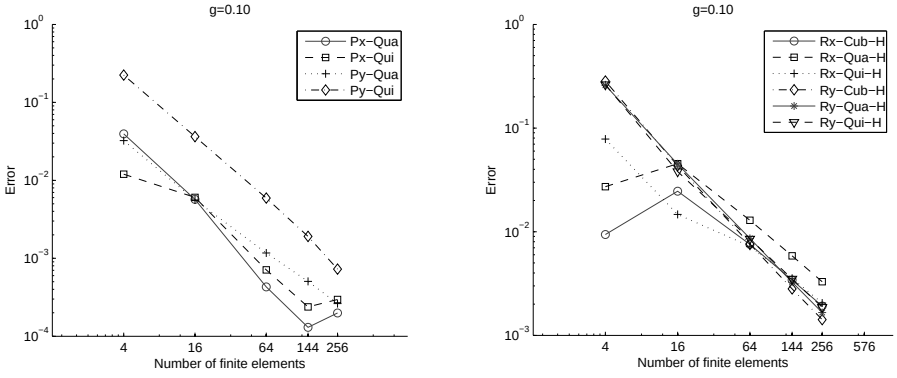

Figure 4: For $g = 0.1$, errors in the evaluation of classical forces at the center node of the parallelogram, on the left, as well as of the sum of non-classical forces on the horizontal edges at the same point.

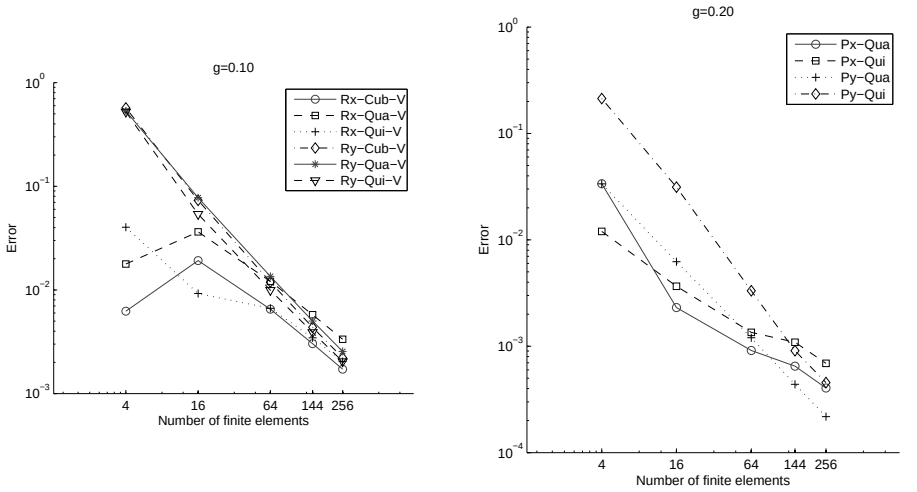

Figure 5: Left: Errors in the evaluation of the sum of non-classical forces ate the inclined edges at the center node of the parallelogram, for $g = 0.1$, on the left, as well as in the evaluation of classical forces, for $g = 0.2$.

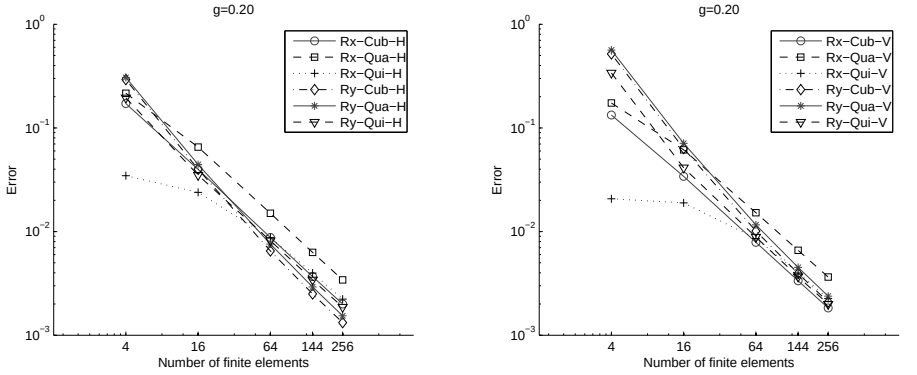

Figure 6: Errors in the evaluation of the sum of non-classical forces at the center node of the parallelogram on the horizontal as well as on the inclined edges, for $g = 0.2$.

7.1.2 Convergence tests for the evaluation of edge forces

For the same example of the previous Section, the balance of forces at the central node on the right edge of the parallelogram is investigated. The error norm is

$$error(p_i) = \frac{|\mathbf{Kd} - \mathbf{p}|}{|\mathbf{Kd}|} \tag{59}$$

where $\mathbf{K}$ is the stiffness matrix defined in Eq. (38), $\mathbf{d}$ are nodal displacements and gradient displacements corresponding to the applied polynomial fields and the equivalent nodal forces $\mathbf{p}$ are defined as in Eq. (34) for boundary traction values obtained as illustrated in Eqs. (53)-(55) for the cubic polynomial. Figure 7 shows on the left the convergence pattern one should expect according to the classical elasticity theory. The results on the right of Fig. 7 and left of Fig. 8 are the convergence studies carried out for $g = 0.1$ and $g = 0.2$. Only results related to the "classical" forces in the horizontal direction (P_x) are ploted, recalling that they correspond to the upper subvector of $\mathbf{p}$ in Eq. (34). The convergence pattern is no longer a straight line in the loglog graphics. The same results, now accrued by values for $g = 0.3$, are

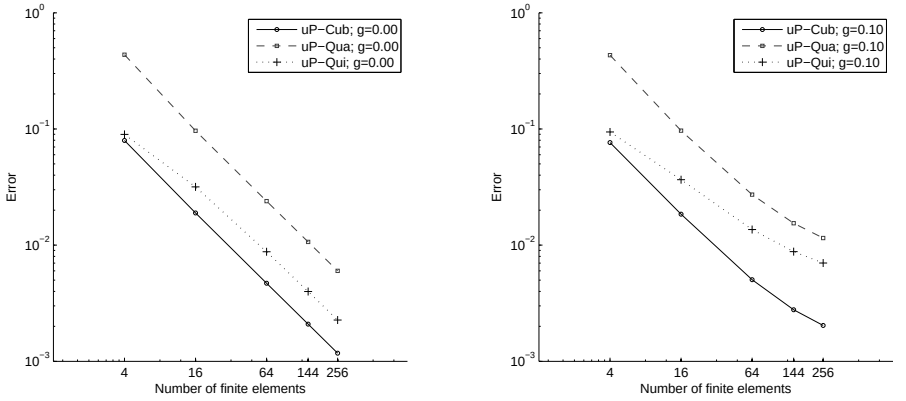

Figure 7: Errors in the evaluation of classical forces at the center node on the right edge of the parallelogram of Fig. 3, for $g = 0$ and $g = 0.1$.

grouped on the right of Figs. 8 and 9 for each polynomial field. Increasing values of g lead to slower convergence patterns, which is unwanted and actually frustrates the author's expectations. These results are still under analysis, but a possible explanation is related to the interpretation of the equivalent boundary forces, to which values obtained for all edges concurring in the nodal point should contribute. On the other hand, this convergence pattern is not inedited in the technical literature [see Zervos, Papanicolopulos, and Vardoulakis (2009), for instance].

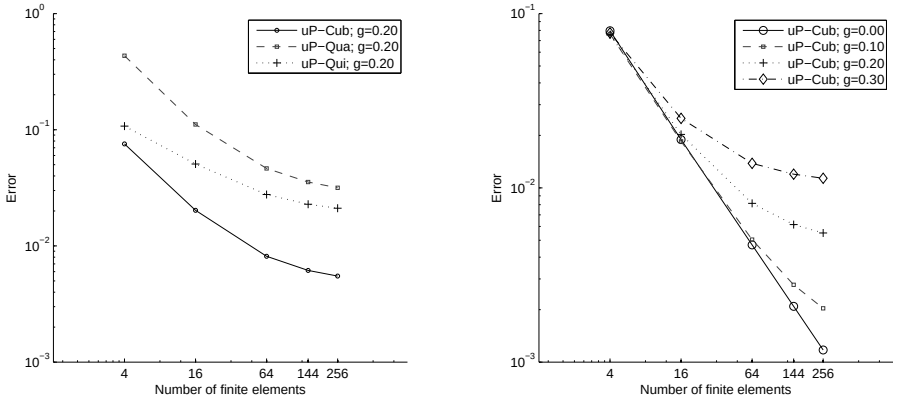

Figure 8: Errors in the evaluation of classical forces at the center node on the right edge of the parallelogram, for $g = 0.2$, on the left, as well as comparison of the results for different values of g, grouped for the cubic displacement field.

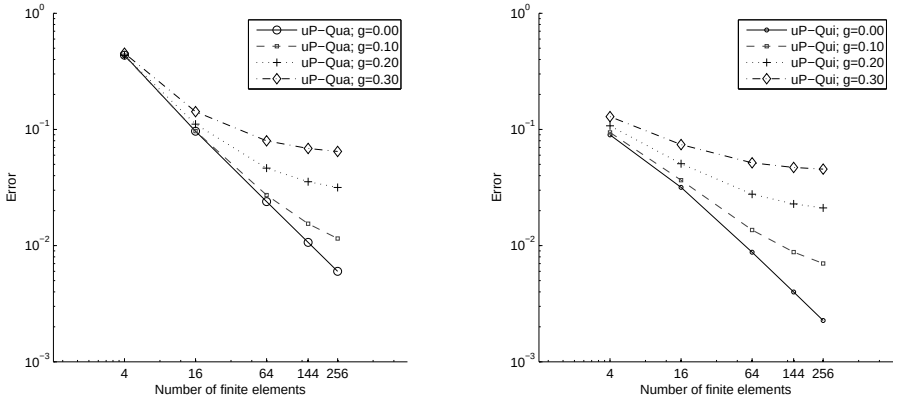

Figure 9: Errors for different values of g, grouped for the quartic and quintic displacement fields.

7.2 A convergence test for quadratic quadrilateral elements

Another series of tests was carried out for a square-shaped elastic body shown on the left of Fig. 10, using 2×2, 4×4, 8×8 or 12×12 quadratic quadrilateral elements (elements Q8 of Table 1), with corresponding 98, 338, 1250 or 2738 degrees of freedom. Figure 11 shows several convergence results at the center node of the square body, for the error norm shown in Eq. (58), with the values of all non-classical (R_i) forces adjacent to the node added as a single result. Maybe as a result of the simple, square-shaped solid, the observed convergence pattern has turned out by far better the in the previous examples.

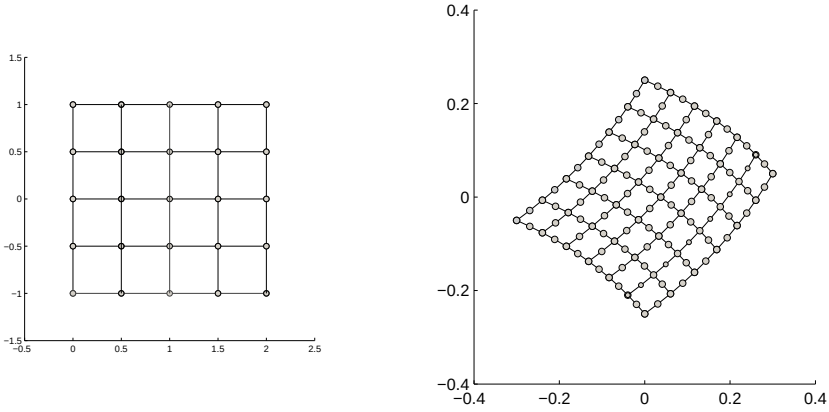

Figure 10: Left: Square-shaped elastic body modeled with either 4, 16, 64 or 144 quadratic quadrilateral elements. Right: Curved elastic body modeled with either 16, 36, 64 or 100 quadratic quadrilateral elements.

7.3 A convergence test for curved quadratic quadrilateral elements

An elastic body with 6×6 curved quadratic elements is shown on the right of Fig. 10. In a convergence test, this solid is discretized with either 4×4, 6×6, 8×8 or 10×10 elements. Since an edge node has four dof and a corner node six dof, the corresponding total number of dof for each discretization case is 418, 818, 1362 or 2050, respectively. Besides the cubic, quartic and quintic of Eqs. (52)-(57), this solid is submitted to one linear and two different quadratic fields, represented by the columns of the matrix

$$u_i{}^p = \begin{bmatrix} x(-5+8\nu) & (-1+2\nu)x^2+2(1-\nu)y^2 & 2xy(-3+4\nu) \\ y & 0 & x^2+y^2 \end{bmatrix} \tag{60}$$

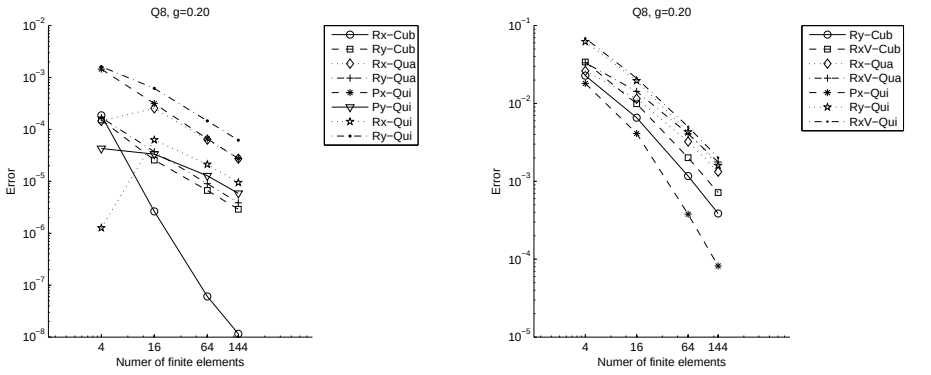

Figure 11: Errors for classical and non-classical forces evaluated for the center node of a square solid discretized with quadratic elements.

The convergence results for classical and non-classical forces at the central node of the solid, according to the error norm of Eq. (59) and as described in previous examples, are displayed in Figs. 12 and 13. Once more, excellent convergence pattern is observed, showing consistency of the whole formulation.

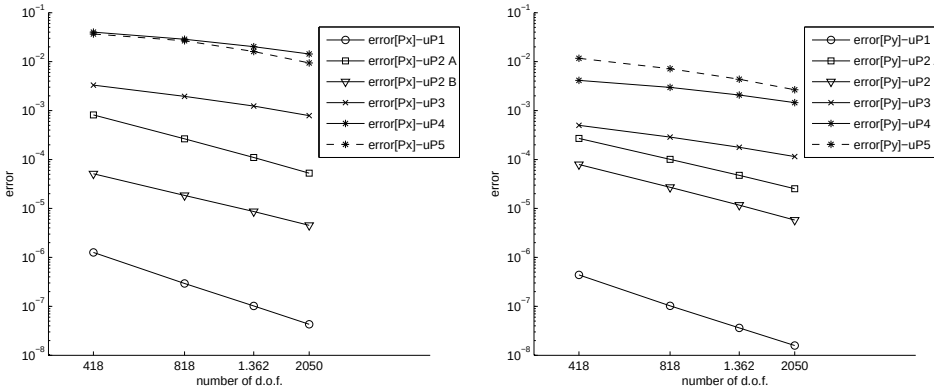

Figure 12: Convergence results for the evaluated classical nodal forces at the central node of the irregular solid of Fig. 10.

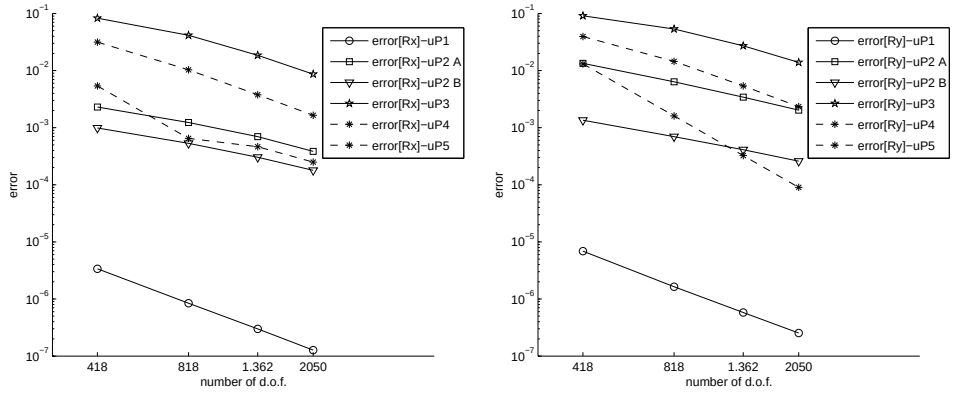

Figure 13: Convergence results for the evaluated non-classical nodal forces at the central node of the irregular solid of Fig. 10.

8 Concluding remarks

The present developments consolidate several years of research in the frame of the second author's M.Sc. and Ph.D works [Huamán (2013)], with results already partially presented in some conferences, but brought together for the first time as a publishable manuscript. This paper presents a concise hybrid finite/boundary element formulation of gradient elasticity problems based on two virtual work principles that stem from the Hellinger-Reissner potential. General non-singular fundamental solutions – the homogeneous solutions of Eq. (5) – are derived in a comprehensive framework [Huamán (2013)]. An important contribution is the variational evidence that the proposed hybrid formulation naturally approximates normal displacement gradients along the boundary Γ independently from displacements, which is a step forward from the proposition made by Mindlin and Eshel (1968) on the basis of a single displacement field. This assumption is in consonance with the proposition by Polyzos, Tsepoura, Tsinopoulos, and Beskos (2003) in the frame of the collocation boundary element method. The finite element implementation of gradient elasticity requires a huge number of degrees of freedom, as compared with the classical elasticity [and as compared with a skilled meshless implementation, according to Tang, Shen, and Atluri (2003)], and the computational developments still lack a complete mechanical interpretation. Consistency of the formulation as well as convergence of some key numerical results could be systematically assessed for a series of patch tests that also have made possible to correlate external and internal non-classical quantities. Then, although meaningful non-classical boundary conditions are still difficult to understand and establish, the authors hope to have contributed to the

improvement of this delicate research area. The next step is the application of the developed numerical tool to problems actually tested in the laboratory. The basic developments outlined in this paper are directly applicable to a boundary element formulation. In this case, the displacement fundamental solution of the problem, for linear gradient elasticity, is non-singular, but the solution related to the total stresses is singular, while the non-classical forces require dealing with hypersingular integrals [Polyzos, Tsepoura, Tsinopoulos, and Beskos (2003)]. All these peculiarities are being prepared for publication in a companion paper.

Acknowledgments

This project was supported by the Brazilian agencies CAPES, CNPq and FAPERJ.

References

Aifantis, E. C. (2009): Exploring the applicability of gradient elasticity to certain micro/nano reliability problems. *Microsystem Technologies*, vol. 15, pp. 109–115.

Aifantis, E. C. (2011): On the gradient approach - relation to Eringen's nonlocal theory. *International Journal of Engineering Science*, vol. 49, pp. 1367–1377.

Amanatidou, E.; Aravas, N. (2002): Mixed finite element formulations of strain-gradient elasticity problems. *Computer Methods in Applied Mechanics and Engineering*, vol. 191, pp. 1723–1751.

Challamel, N.; Wang, C. M. (2008): The small length scale effect for non-local cantilever beam: a paradox solved. *Nanotechnology*, vol. 19, no. 34, pp. 7pp.

Cosserat, E.; Cosserat, F. (1909): *Théorie des Corps Déformables*. A. Hermann & Fils.

Dumont, N. A. (1989): The hybrid boundary element method: an alliance between mechanical consistency and simplicity. *Applied Mechanics Reviews*, vol. 42, no. 11, pp. S54–S63.

Dumont, N. A. (2003): Variationally-based hybrid boundary element methods. *Computer Assisted Mechanics and Engineering Sciences*, vol. 10, pp. 407–430.

Dumont, N. A. (2005): An advanced mode superposition technique for the general analysis of time-dependent problems. In Selvadurai, A. P. S.; Tan, C. L.; Aliabadi, M. H.(Eds): *BETeq 2005 - 6th International Conference on Boundary Element Techniques*, pp. 333–344, Montreal, Canada. CL Ltd.

Dumont, N. A. (2007): On the solution of generalized non-linear complex-symmetric eigenvalue problems. *International Journal for Numerical Methods in Engineering*, vol. 71, pp. 1534–1568.

Dumont, N. A.; Aguilar, C. A. (2009): Linear algebra issues in a family of advanced hybrid finite elements. In *CMAS2009 - Computational Modelling and Advanced Simulations*, 15 pp, Bratislava, Eslovac Republic. ECCOMAS.

Dumont, N. A.; Huamán, D. (2009): Hybrid finite/boundary element formulation for strain gradient elasticity problems. In Sapountzakis, E. J.; Aliabadi, M. H.(Eds): *BETeq 2009 - International Conference on Boundary Element Techniques*, pp. 295–300, Athens, Greece.

Dumont, N. A.; Huamán, D. (2010): A family of 2D and 3D hybrid finite elements for strain gradient elasticity. In Zhang, C.; Aliabadi, M. H.; Schanz, M.(Eds): *Advances in Boundary Element Techniques XI, Proceedings of the 11th International Conference*, pp. 144–153, Berlin, Germany.

Dumont, N. A.; Huamán, D. (2010): A hybrid finite element implementation of gradient elasticity. In *11th Pan-American Congress of Applied Mechanics - PACAM XI*, pg. 6 pp, Foz do Iguaçu, Brazil.

Dumont, N. A.; Prazeres, P. G. C. (2005): Hybrid dynamic finite element families for the general analysis of time-dependent problems. In *ICSSD 2005 - Third International Conference on Structural Stability and Dynamics*, 10 pp on CD, Kissimee, Florida. ICSSD.

Ericksen, J.; Trusdel, C. (1958): Exact theory of stress and strain in rods and shells. *Archive for Rational Mechanics and Analysis*, vol. 1, pp. 295–323.

Eringen, A. C. (1972): Nonlocal polar elastic continua. *International Journal of Engineering Science*, vol. 10, pp. 1–16.

Giannakopoulos, A. E.; Amanatidou, E.; Aravas, N. (2006): A reciprocity theorem in linear gradient elasticity and the corresponding Saint-Venant principle. *International Journal of Solids and Structures*, vol. 43, pp. 3875–3894.

Gourgiotis, P. A.; Georgiadis, H. G. (2009): Plane-strain crack problems in microstructured solids governed by dipolar gradient elasticity. *Journal of the Mechanics and Physics of Solids*, vol. 57, pp. 1898–1920.

Gourgiotis, P. A.; Sifnaiou, M. D.; Georgiadis, H. G. (2010): The problem of sharp notch in microstructured solids governed by dipolar gradient elasticity. *International Journal of Fracture*, vol. 166, pp. 179–201.

Grentzelou, C. G.; Georgiadis, H. G. (2008): Balance laws and energy release rates for cracks in dipolar gradient elasticity. *International Journal of Solids and Structures*, vol. 45, pp. 551–567.

Huamán, D. (2013): *The Hybrid Boundary Element Method Applied to Gradient Elasticity Problems*. Ph.D. thesis, PUC-Rio, Rio de Janeiro, Brazil, 2013.

Huamán, D. (2014): *Some Finite Element Applications in Gradient Elasticity*. Internal report, PUC-Rio, Rio de Janeiro, Brazil, 2014.

Kahrobaiyan, M. H.; Asghari, M.; Rhaeifard, M.; Ahmadian, M. T. (2011): A nonlinear strain gradient beam formulation. *International Journal of Engineering Science*, vol. 49, pp. 1256–1267.

Kreyszig, E. (1991): *Differential Geometry*. Dover, New York.

Maranganti, R.; Sharma, P. (2007): A novel atomistic approach to determine strain-gradient elasticity constants: Tabulation and comparison for various metals, semiconductors, silica, polymers and the (ir)relevance for nanotechnologies. *Journal of the Mechanics and Physics of Solids*, vol. 55, pp. 1823–1852.

Mindlin, R. D. (1964): Micro-structure in linear elasticity. *Archive for Rational Mechanics and Analysis*, vol. 16, pp. 51–78.

Mindlin, R. D.; Eshel, N. N. (1968): On first strain gradient theories in linear elasticity. *International Journal of Solids and Structures*, vol. 4, pp. 109–124.

Nikolov, S.; Han, C. S.; Raabe, D. (2007): On the origin of size effect in small-strain elasticity of solid polymers. *International Journal of Solids and structures*, vol. 44, pp. 1582–1592.

Papargyri-Beskou, S.; Beskos, D. E. (2008): Static, stability and dynamic analysis of gradient elastic flexural kirchhoff plates. *Archive of Applied Mechanics*, vol. 78, pp. 625–635.

Papargyri-Beskou, S.; Beskos, D. E. (2009): Static analysis of gradient elastic circular cylindrical thin shells. *International Journal of Engineering Science*, vol. 47, pp. 1379–1385.

Papargyri-Beskou, S.; Polyzos, D.; Beskos, D. E. (2009): Wave dispersion in gradient elastic solids and structures: A unified treatment. *International Journal of Solids and Structures*, vol. 46, pp. 3751–3759.

Peerlings, R. H. J.; Fleck, N. A. (2004): Computational evaluation of strain gradient elasticity constants. *International Journal for Multiscale Computational Engineering*, vol. 2, no. 4, pp. 599–619.

Polyzos, D.; Tsepoura, K. G.; Tsinopoulos, S. V.; Beskos, D. E. (2003): A boundary element method for solving 2-D and 3-D static gradient elastic problems part I: Integral formulation. *Computer Methods in Applied Mechanics and Engineering*, vol. 192, pp. 2845–2873.

Reddy, J. N. (2007): Nonlocal theories for bending buckling and vibration of beams. *International Journal of Engineering Science*, vol. 45, pp. 288–307.

Sciarra, F. M. D. (2009): On non-local and non-homogeneous elastic continua. *International Journal of Solids and Structures*, vol. 46, pp. 651–676.

Sellountos, E. J.; Tsinopoulos, S. V.; Polyzos, D. (2012): A LBIE method for solving gradient elastostatic problems. *CMES: Computer Modeling in Engineering & Sciences*, vol. 86, no. 2, pp. 145–169.

Tang, Z.; Shen, S.; Atluri, S. N. (2003): Analysis of materials with strain-gradient effects: A meshless local Petrov-Galerkin MLPG approach, with nodal displacements only. *CMES: Computer Modeling in Engineering & Sciences*, vol. 4, no. 1, pp. 177–196.

Toupin, R. A. (1962): Elastic materials with couple stresses. *Archive for Rational Mechanics and Analysis*, vol. 11, pp. 385–414.

Tsepoura, K. G.; Papargyri, S.; Polyzos, D.; Beskos, D. E. (2002): Static and dynamic analysis of a gradient-elastic bar in tension. *Applied Mechanics*, vol. 72, pp. 483–497.

Tsinopoulos, S. V.; Polyzos, D.; Beskos, D. E. (2012): Static and dynamic BEM analysis of strain gradient elastic solids and structures. *CMES: Computer Modeling in Engineering & Sciences*, vol. 86, no. 2, pp. 113–144.

Zervos, A.; Papanicolopulos, S.-A.; Vardoulakis, I. (2009): Two finite-element discretizations for gradient elasticity. *Journal of Engineering Mechanics*, vol. 135, pp. 203–213.